

MODELING A THREE FILAMENT PLASMA EXPERIMENT WITH AN ADAPTED SINGLE FILAMENT MODEL

Miles Kent, XXXXXXX

Department of Physics, University of Alberta, Edmonton, AB, T6G 0C7

Abstract

A model describing a single temperature filament was derived in a recent study (Shi et al. 2009) to explore the results of a single filament plasma experiment. We adapt this model to represent a three-filament experiment, testing the model's ability to describe experiments with higher filament numbers. A numerical study is preformed using the adapted three-filament model where the temperature dispersion and flow fields are analyzed for unimodal and bimodal structures. The results of this numerical study are compared to data from a recent three-filament experiment (Sydora et al, 2019), testing the model's ability to be represent experiments with higher filament numbers. Lastly, we will discuss how to make the model more accurate based on the results of comparing the data.

Introduction

Temperature filaments are a widely studied phenomena in plasma science. A temperature filament is defined as a structure in a magnetized plasma that is much longer in length than in width (Shi et al. 2009), which is created by a heat source imposed in a plasma medium (Shi et al 2009). The heat source causes movement in the plasma due to diffusion and convection, generating structures that are often unique (Sydora et al. 2019). Due to their complexity, modeling the properties of a filament structure can be a formidable task.

A single temperature filament was modeled in a recent study (Shi et al. 2009). This model was used to investigate the results of a single filament plasma experiment performed on the LAPD (Large Plasma device) (Pace et al. 2008, Burk et al. 2000), where a temperature filament was created by a stream of electrons with no curvature injected into a cold helium plasma along a uniform magnetic field (Burk et al 2000). The single filament model considered classical heat transport equations (see Shi et al. 2009) in its formulation, leading to an oscillatory solution describing ideal drift waves and convective flows in the plasma medium (Shi et al. 2009). The base of the single filament model is a potential waveform described by the superposition of radial Bessel function (Shi et al. 2009), represented by **(1)** (Shi et al. 2009). This waveform equation allows us to explore the convective flows and temperature distributions in a filament, where positive polarity correlates to heated flows while a negative polarity correlates to cooler flows (Shi et al. 2009). The field strength of this potential can be extracted from this potential equation by differentiating the equation. From this calculation, we can derive the local flow velocity allowing us to define a convective flow field to analyze the movement in the plasma.

In this study, the single filament model is adapted to represent a three-filament plasma experiment performed on the Large Plasma Device (LAPD). Data was collected for three electron temperature filaments in a triangular formation placed 0.5cm from each other (Sydora et al. 2019). This was repeated for the filaments located 1.5cm from each other (Sydora et al. 2019). A numerical study is conducted at both distances where the adapted model is simulated for a $2\mu\text{s}$ interval corresponding to the time step of many LAPD experiments (Shi et al 2009). The result of this numerical study is presented and compared to experimental data to test how well the adapted three filament model can describe a three-filament experiment. We will discuss how to improve the model to make it more accurate in determining results.

Experiment setup

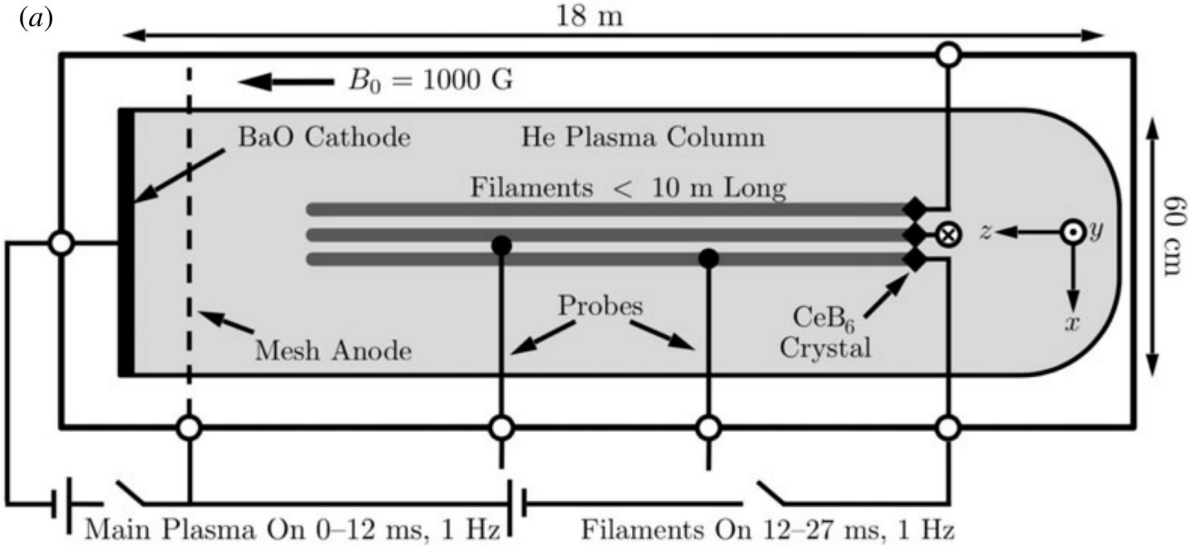


Figure 1: Experimental set up of the upgraded large plasma device (not to scale) with three filaments located in a triangular formation. Figure from Sydora et al. 2019.

The single filament model is adapted to represent the three-filament experiment (see Sydora et al. 2019) performed on the LAPD (upgraded large plasma device) (Figure 1). This experiment consists of a long confined cylindrical helium plasma column (18m by 60cm diameter) magnetized by a uniform magnetic field of 0.1 Tesla along the z axis (Figure 1). The confined plasma is created by collisional ionization from electrons fired at a pulsating rate of 1Hz from a large Barium Oxide (BaO) cathode (Sydora et al. 2019). Three Cerium Hexaboride (CeB_6) crystals arranged in triangular formation opposite of the BaO cathode fire electrons in a straight line along the uniform magnetic field into the plasma creating temperature filaments (Sydora et al. 2019). These filaments energize the surrounding plasma and causing movement due to diffusion and convection (Sydora et al. 2019). The three cathodes can be moved radially from the center and rotated in the triangle formation allowing us to analyze the behavior of the temperature filaments in the magnetized plasma column for many different filament orientations. The experiment was conducted in the afterglow phase of the helium plasma which last for about 100 μs just after each pulse of the BaO cathode. Data was collected using Langmuir probes that can be moved along the x y plane in intervals of 23cm distance down the length of the tube (Sydora et al 2019). I will focus on data collected at filament distances 0.5 cm and 1.5 cm at 290cm down the length of the tube and the potential and ion saturation current data recorded in this experiment.

Model derivation and formalism

Single filament potential model

The single filament potential is scalar potential model representing the properties of a temperature filament on a 2D polar plane perpendicular to a uniform magnetic field. This potential generates a waveform where positive modes describe hot flows while negative modes describe cooler flows.

$$\delta(r, \theta, t) = A_1 J_1(k_1 r) e^{im_1 \theta} e^{-\alpha r} e^{-iwt} + A_6 J_6(k_6 r) e^{im_6 \theta} e^{-\alpha r} e^{-iwt} \quad (1)$$

The single filament potential is represented (1) which is the superposition of two radial Bessel functions J_n with indices 1 and 6. The indices represent the mode number of each Bessel function. The single filament potential is extremely malleable allowing us to modify the oscillation frequency w , the damping coefficient, α , the mode number, m , the wave number, k , and the mode amplitude, A . This allows the single filament potential to be widely applicable to many different filament structures. To represent the three-filament experiment (Sydora et al. 2019), we set A_6 to zero due to the absence of an external six-mode structure (seen in Shi et al. 2009) observed in the data. Our model becomes

$$\delta(r, \theta, t) = A_n J_n(k_n r) e^{im_n \theta} e^{-\alpha r} e^{-iwt} \quad (2)$$

because of this modification. We also include a flexible mode number “ n ” instead of permanently setting the mode number to one to make the model more applicable to our experiment

Single filament flow field

The flow field can be calculated uniformly to Shi et al 2009, where plasma is assumed to follow a flow field derived from the Shi potential. We can calculate the field strength in the r and θ direction from our modified Shi potential using (3) where p is the coordinate parameter of focus.

$$\mathbf{E} = -\frac{\partial \delta}{\partial p} \quad (3)$$

The resulting fields in the r and θ direction are represented by (4) and (5).

$$E_r(r, \theta, t) = -A_1 \left(\frac{\partial J_1(k_1 r)}{\partial r} - \alpha J_1(k_1 r) \right) e^{im_1 \theta} e^{-\alpha r} e^{-iwt} \quad (4)$$

$$E_\theta(r, \theta, t) = -\frac{im_1}{r} A_1 J_1(k_1 r) e^{im_1 \theta} e^{-\alpha r} e^{-iwt} \quad (5)$$

The fields can be represented in the x and y directions using (6) and (7).

$$E_x = E_r \cos \theta - E_\theta \sin \theta \quad (6)$$

$$E_y = E_r \sin \theta + E_\theta \cos \theta \quad (7)$$

The local flow velocity in the x and y direction can be expressed by vectors using (8) and (9)

$$\mathbf{U} = \frac{E_y}{B} \quad (8)$$

$$\mathbf{V} = \frac{E_x}{B} \quad (9)$$

where \mathbf{B} is the magnetic field strength. This uniform magnetic field strength is set to 0.1 T for the three-filament experiment.

Cartesian representation of single filament model and flow field

The adapted single filament model needs to be represented on a 2D cartesian plain to effectively model the three-filament plasma experiment. The scalar potential and plasma flow field can be represented with cartesian coordinates by substituting (10) and (11) into (2), (4), and (5).

$$r = \sqrt{x^2 + y^2} \quad (10)$$

$$\theta = \tan^{-1} \left(\frac{y}{x} \right) \quad (11)$$

The frame of reference of the single filament potential model can be changed by centering it at different points on the cartesian plane. (10) and (11) are modified to represent a change of frame where x' and y' represent new origin location of the model on the cartesian plane. (12) and (13) are the resulting equations substituted into the model.

$$r = \sqrt{(x - x')^2 + (y - y')^2} \quad (12)$$

$$\theta = \tan^{-1} \left(\frac{y - y'}{x - x'} \right) \quad (13)$$

Three filament model

The three-filament model is composed of the sum of three individual potentials sitting in three different frames of reference on the cartesian plane. The total field total field potential is represented by

$$\delta(x, y, t) = \sum_{n=1}^3 \delta_n \left\{ r \left((x - x'_n), (y - y'_n) \right), \theta \left((x - x'_n), (y - y'_n) \right), t \right\} \quad (14)$$

where (12) and (13) have been substituted into (2). The center point of each potential is represented by individual points x'_n and y'_n . Using the same formalism, (4) and (5) become

$$E_x(x, y, t) = \sum_{n=1}^3 E_{xn} \left\{ r \left((x - x'_n), (y - y'_n) \right), \theta \left((x - x'_n), (y - y'_n) \right), t \right\} \quad (15)$$

$$E_y(x, y, t) = \sum_{n=1}^3 E_{yn} \left\{ r \left((x - x'_n), (y - y'_n) \right), \theta \left((x - x'_n), (y - y'_n) \right), t \right\} \quad (16)$$

(8) and (9) become a sum of vectors represented by

$$\mathbf{U} = \sum_{n=1}^3 \frac{E_{nx}}{B} \quad (17)$$

$$\mathbf{V} = \sum_{n=1}^3 \frac{E_{ny}}{B} \quad (18)$$

Adapting the three-filament model

The model can be adjusted to mimic the triangular formation of filaments in the experiment. The model can also be adjusted to operate uniformly to the LAPD where a filament proximity can be modified by a distance, d , as well as a formation rotation angle, θ_{in} , which describes the angle of rotation of the triangle filament formation. This is done by defining a parameter R which represents the uniform filament distance from the origin of the cartesian plane as a function of d

$$R = \frac{d}{\sqrt{3}} \quad (18)$$

(18) allow us to move each filament a distance from the center when placed into

$$x'(d, \theta_{in}) = R(d) \cos(\theta_{in} + \theta_n) \quad (19)$$

$$y'(d, \theta_{in}) = R(d) \sin(\theta_{in} + \theta_n) \quad (20)$$

Where θ_n represents the azimuthal distance that each filament is initially located from $x=0$ on the cartesian plane. n represents the filament number. The triangular structure displayed by the LAPD can be formulated by setting $\theta_1 = 0$, $\theta_2 = \frac{2\pi}{3}$, and $\theta_3 = \frac{4\pi}{3}$, for each corresponding filament. Substituting (19) and (20) into (14), (15), and (16), the three-filament potential reaches the desired form.

$$\delta(x, y, t) = \sum_{n=1}^3 \delta_n \left\{ r \left((x - x'_n(d, \theta in, \theta_n)), (y - y'_n(d, \theta in, \theta_n)) \right), \theta \left((x - x'_n(d, \theta in, \theta_n)), (y - y'_n(d, \theta in, \theta_n)) \right), t \right\} \quad (21)$$

Using the same formalism, (15) and (16) become

$$E_x(x, y, t) = \sum_{n=1}^3 E_{xn} \left\{ r \left((x - x'_n(d, \theta in, \theta_n)), (y - y'_n(d, \theta in, \theta_n)) \right), \theta \left((x - x'_n(d, \theta in, \theta_n)), (y - y'_n(d, \theta in, \theta_n)) \right), t \right\} \quad (22)$$

$$E_y(x, y, t) = \sum_{n=1}^3 E_{yn} \left\{ r \left((x - x'_n(d, \theta in, \theta_n)), (y - y'_n(d, \theta in, \theta_n)) \right), \theta \left((x - x'_n(d, \theta in, \theta_n)), (y - y'_n(d, \theta in, \theta_n)) \right), t \right\} \quad (23)$$

Where the sum of vectors for **U** and **V** is represented by (17) and (18) but with (22) and (23) as the **E** terms.

Numerical study

A numerical study was conducted for the three-filament model for model mode numbers zero (Figure 2) and one (Figure 3) where we created a simulation of our model for a $2\mu\text{s}$ interval to analyze how the temperature filaments behave when described by the three-filament model. The numerical was performed for filament distances of 0.5cm and 1.5cm from each other, which was uniform to the data collected in the experiment. To accurately display the radical localization of modes observed in the experiment, we have set the damping coefficient to a value that makes the modes outside of the first oscillation negligible (Sydora et al. 2019). The mode amplitude was normalized in all models to give a uniform amplitude to all calculations.

Single mode model

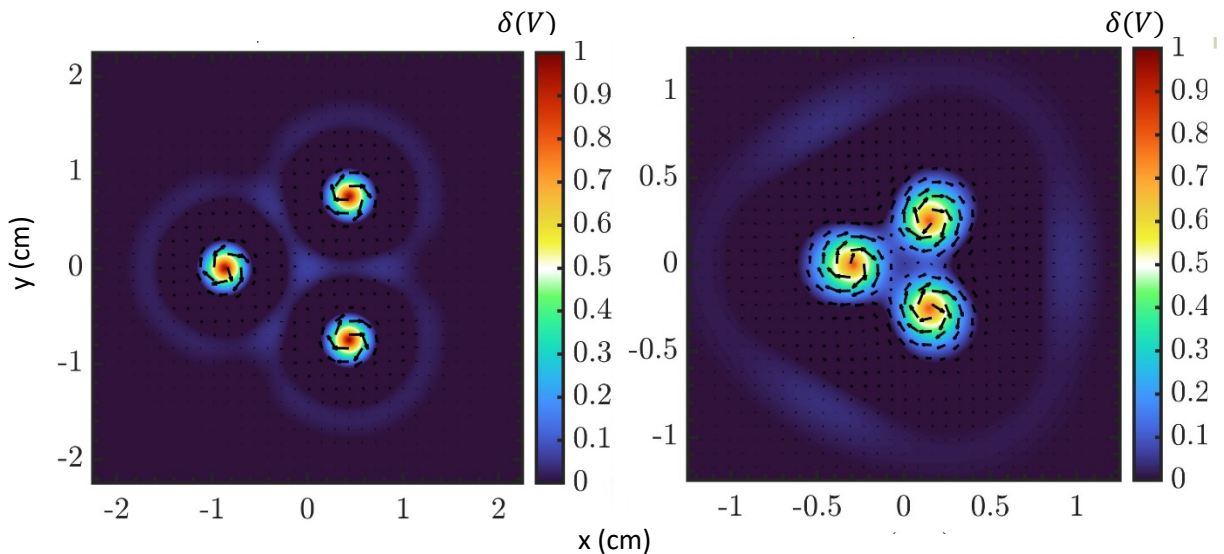


Figure 2: Three filament potential model with an overlying vector field representing the flow field for $\mathbf{m} = 0$ at distances 1.5cm (left) and 0.5cm (right).

A numerical model for a single filament mode structure ($\mathbf{m} = 0$) was generated (Figure 2) for filament distances 1.5cm (left) and 0.5 cm (right) (Figure 2). The single mode has a max amplitude at the center of each filament location, corresponding the maximum temperature at the center of the filament. An azimuthally symmetric plasma flow field is generated around each heated filament rotating clockwise corresponding to the steep temperature gradient created by the filament. The potential range has been from 0 to 1 V allowing a clear view of the temperature gradient and the azimuthally symmetric mode structure.

Bimodal model

A numerical model for a bimodal filament structure ($\mathbf{m} = 1$) was generated (Figure 3) for filament distances 1.5cm (left) and 0.5 cm (right). Opposing temperature gradients are observed adjacent

to each other around the center of the filament location. The temperature gradients create convective flow fields in opposing directions forming dipole structures in the plasma.

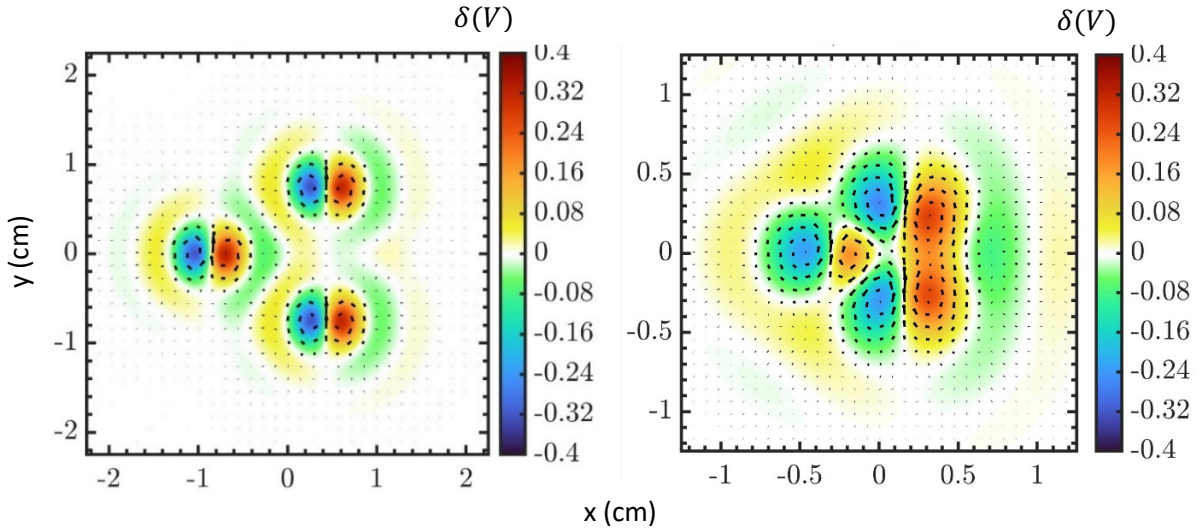


Figure 3: Three filament potential model with an overlying vector field representing the flow field for $\mathbf{m} = 0$ at distances 1.5cm (left) and 0.5 (right).

These structures rotate at a frequency of 35 kHz in our simulation corresponding to convection observed in our model. The mode structures mix when the filaments are placed 0.5cm from each other (left) creating unique temperature dispersions in the plasma which results in flow vortices that stretch and compress with time. We set the potential window to be from -.4 to .4 V so the modes can be observed for a normalized potential.

Single mode model with an imposed background potential

A background potential is observed in experimental data when filament structures are placed close together. This background potential has the same polarity as the potential of the filaments it is located around (Figure 4). As a result, we numerically simulated the model of the three-filament potential with an imposed background potential represented by

$$\delta_{br}(r) = C_1 + C_2 e^{-C_3(r-C_4)^2} + C_5(r + 3 \text{ cm})^{-4} \quad (24)$$

where $C_1 = -3.309 \text{ V}$, $C_2 = -0.690 \text{ V}$, $C_3 = 5.712 \text{ cm}^{-2}$, $C_4 = .397 \text{ cm}$, and $C_5 = -75.410 \text{ eV cm}^4$. (24) was derived from the data of the three-filament experiment (observed in Sydora et al. 2019). The negative background potential generates an azimuthal flow field in the counterclockwise direction due to its negative polarity. When the background potential is modeled with the filaments, vortices are created around the filament structures which are superimposed with the curl of the potential (Figure 4). The potential range was set between -4.6 to -3.4 V to observe the gradient in the potential model most clearly.

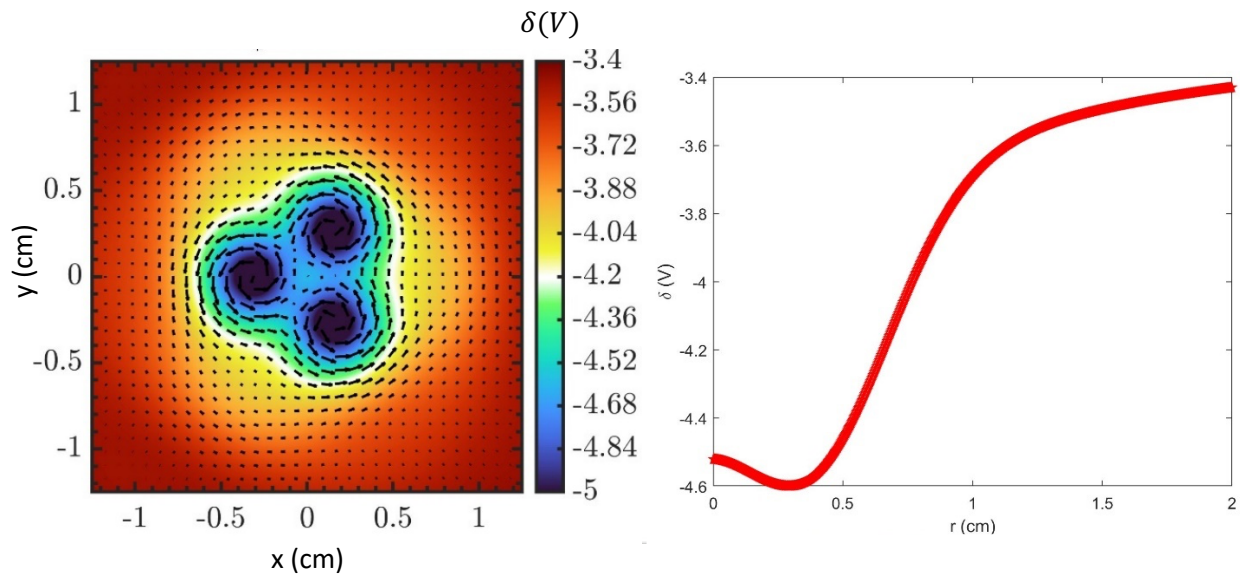


Figure 4: Three filament potential model at 0.5cm distance with the imposed background potential (24) (left). The shape and range of the background potential (right) as a function of r due to the closeness of the filaments.

Comparison and analysis

Comparing potentials

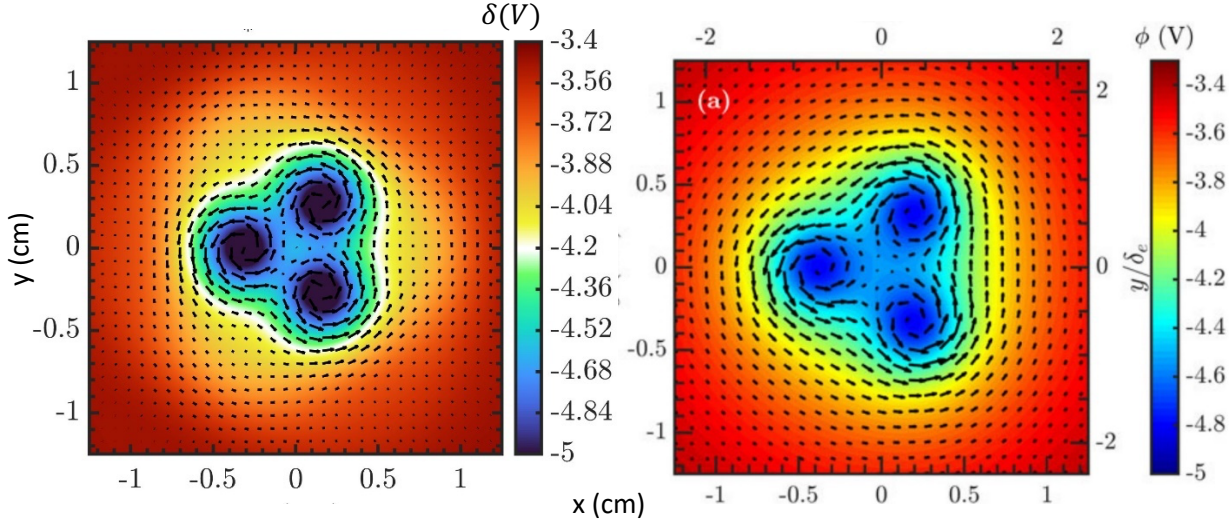


Figure 5: Comparison of the simulation data (left) to the data recorded in the three-filament plasma experiment (right) for a potential range of -5 to -3.4 V.

The numerical study of the three-filament potential with an imposed background potential was compared to the potential observed in the experiment (Figure 5). The three-filament model does a decent job representing the potential data collected in the three-filament experiment, which is observed by the symmetry between the left and right plots. A deviation occurs from the experimental data due to the overall higher mode amplitude displayed by the model. This nonuniformity leads to non-uniform vector amplitudes between the model and the experimental data due to the nonuniformity in the potential magnitude.

Predicting ion saturation current with potential

The predictive power of the three-filament model is tested by comparing the potential to the ion saturation current observed in the experiment. A large ion saturation current amplitude will correlate with a high potential mode value. A single mode structure is observed in the unfiltered data correlating with the observed uniform flow direction. When the data is filtered for wavelengths of 25kHz, we see a dominate bimodal flow structure in the plasma when mapping the current amplitude gradient. This gradient should match with the potential gradient of the adapted three filament model.

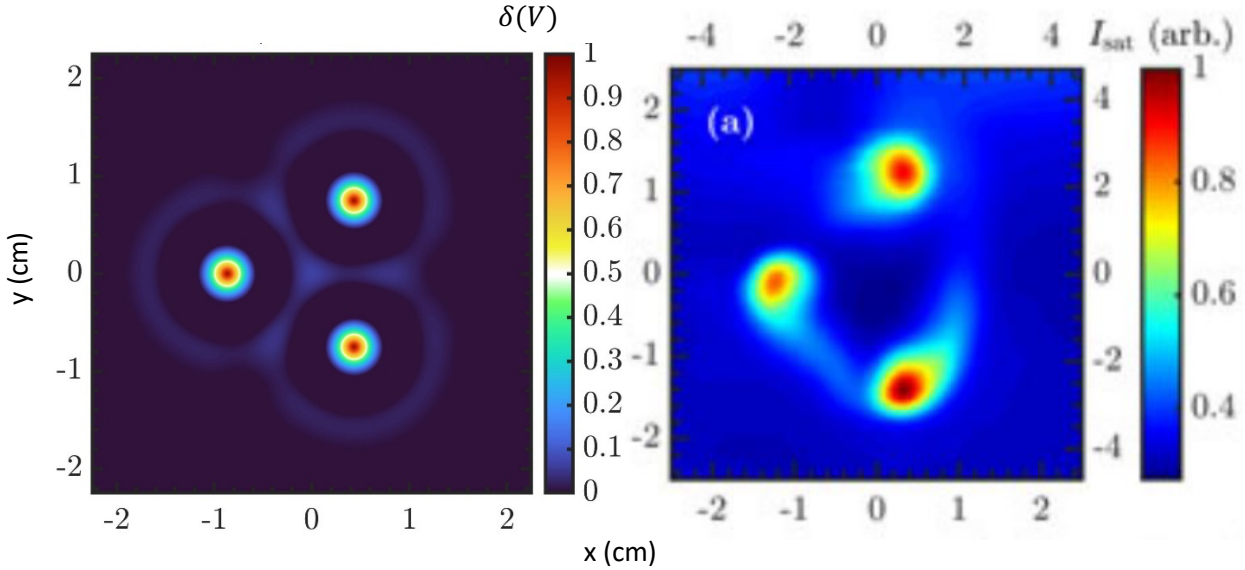


Figure 6: Comparison of the simulation for $m = 0$ (left) and the unfiltered ion saturation current (right) for 1.5cm distance between filaments. The model is in units of volts while the saturation current is in arbitrary units displaying the distribution in magnitude of the saturation current.

The three potential model predicts the ionization current with a high degree of accuracy (Figure 6). The voltage amplitudes match with the ion saturation current amplitudes accurately mapping the steep gradient. The non-uniform size in filament structure in experimental data is due to the non-uniform current observed because of non-uniform voltage which creates a deviation from the three-filament model which assumes uniform mode amplitude. The filaments observed in the experiment appear to have a tail structure which deviates from our model. This may be due to the background energy transfer in the experiment by perpendicular E and B fields of the electron stream and uniform magnetic field (Sydora et al. 2019).

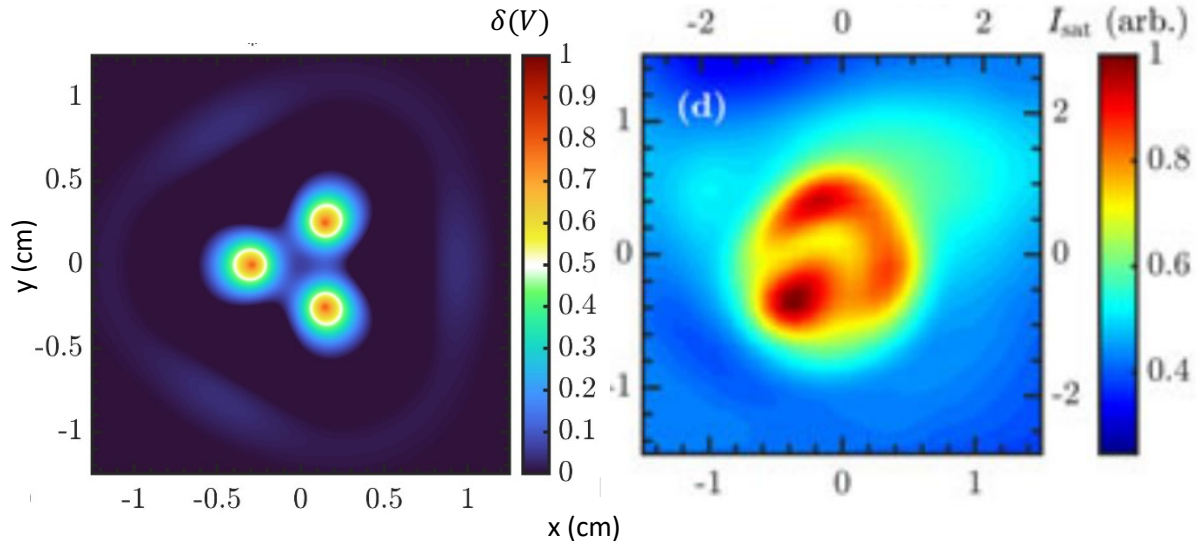


Figure 7: Comparison of the simulation for $\mathbf{m} = 0$ (left) and the unfiltered ion saturation current (right) for 0.5cm distance between filaments. The model is in units of volts while the saturation current is in arbitrary units displaying the distribution in magnitude of the saturation current.

The three potential model does not predict the structure of the ion saturation current nearly as accurately for a close filament distance (Figure 7). This is most likely due to the background potential created by the filaments being close together, which will cause a background ionization current. As a result, an imposed potential model would need to be included as done in the last section to accurately predict the ion saturation current. Another solution is to further modify three-filament potential model to automatically impose a background potential when the filaments are brought close together. This could be done by adding an extra term to the model which decreases with distance.

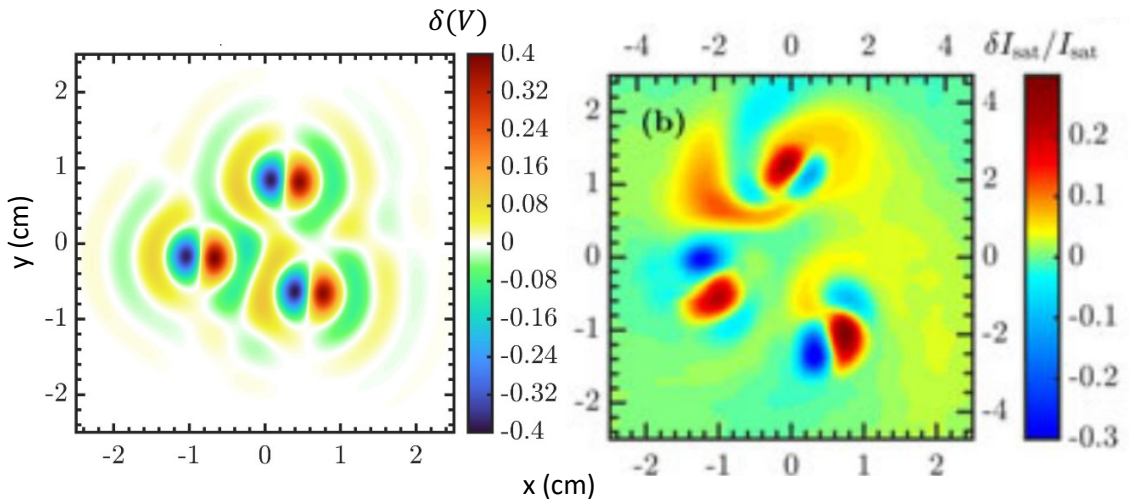


Figure 8: Comparison of the simulation for $\mathbf{m} = 1$ (left) and the filtered ion saturation current (right) for 1.5cm distance between filaments. The model is in units of volts while the saturation current is in arbitrary units displaying the distribution in change in saturation current magnitude

The three-filament model does predict the saturation current gradient with a high degree of accuracy for filtered data at 1.5cm (Figure 8). This is due to the non-uniform number of modes and mode orientations observed between filaments. It is also due to the asymmetry in the mode amplitude and shape of each filament. There is also a tail structure observed on the modes in the data, which are absent in the three-filament model. To model this ion saturation current structure with more accuracy, we need to adapt our model by changing $\mathbf{m} = 2$ for the filament with quad modal structure (bottom right). We also need to add a phase factor to the potential equation allowing us to change the starting orientation of our structures. Even though we can easily make adaptations to describe non uniform mode numbers and orientations, modeling the asymmetry in the individual filament structures is much more difficult due to the symmetric Bessel functions that form the base of the model. The tails could be caused by $\mathbf{E} \times \mathbf{B}$ fields or the rapid spinning of the filament structures which would generate the observed mode skew.

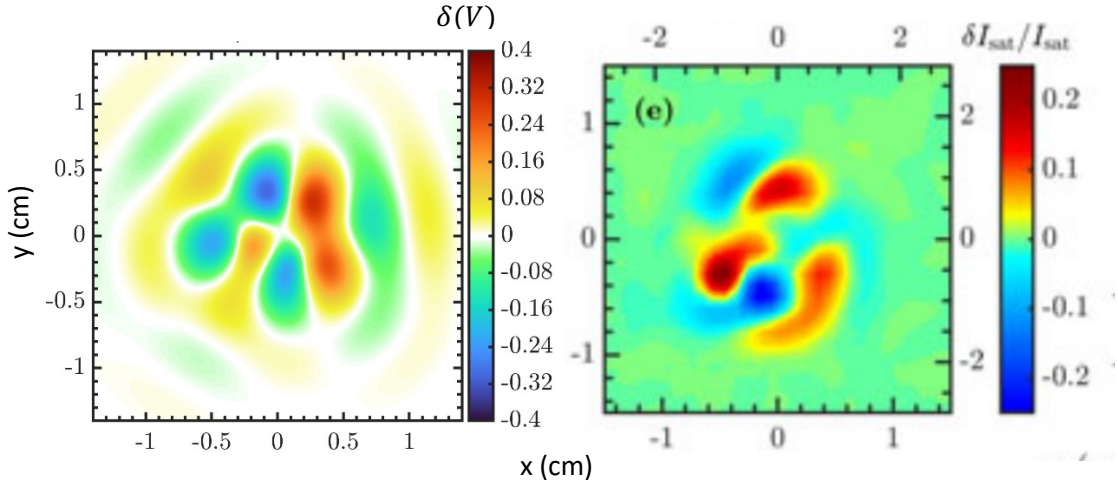


Figure 9: Comparison of the simulation for $m = 1$ (left) and the filtered ion saturation current (right) for 0.5cm distance between filaments. The model is in units of volts while the saturation current is in arbitrary units displaying the distribution in change in saturation current magnitude

The three-filament model does a better job of predicting the ion saturation current at $d = 0.5\text{cm}$. Observed in (Figure 9), the three-filament model can accurately account for the number of modes displayed as well as the mixing of the modes. Where the three-filament model falls short is predicting the size and shape of the interacting mode structures, which could be due to several factors ranging from different mode orientations when mixing to $\mathbf{E} \times \mathbf{B}$ fields.

Summary and conclusion

The three-filament model is successful when modeling the potential in the three-filament plasma experiment. When a background potential model is added to the adapted three filament model to account for the filaments being close together, the adapted three-filament model mimics the experimental potential data almost exactly. The flow fields are accurate in orientation but inaccurate in amplitude due to the difference in filament strength from the data to the model.

The adapted three filament model has varied success in predicting ion saturation current amplitude. The model is extremely successful in predicting single mode structures observed in unfiltered data. This adapted model accurately maps the shape of the structures, the temperature gradient, and resulting plasma flows of the single mode data. On the other hand, the model is much less successful in predicting bimodal structures observed in data filtered by a 25kHz filter. This is a result of the inability for the adapted three filament model to describe non uniform bimodal and quad modal filamentary structures observed in the filtered data due to the design of the model, which only describe symmetric mode structures.

Adjustments can be made to the adapted three filament model to improve its accuracy describing multifilament experiments. One improvement that can be made by adding a phase factor to each oscillatory part of the model, allowing us to model mode structures in different orientations. Another improvement can be made by setting modifiable frequency parameters for each mode equation allowing filaments in the model to rotate at different speeds. We can further modify three-filament potential model to automatically impose a background potential when the filaments are brought close together. This could be done by adding an extra term to the model which decreases with distance.

Overall, the one filament model adapts well to modifications needed to describe higher filament experiments due to its ability to describe mixing structures, flow vortices, and the potential of the experiment. Despite this, the model needs to be further modified to increase its flexibility and accuracy as observed when compared to experimental data.

References

- Sydora, R., Karbaszewski, S., Van Compernolle, B., Poulos, M., & Loughran, J. (2019). Drift-Alfvén fluctuations and transport in multiple interacting magnetized electron temperature filaments. *Journal of Plasma Physics*, *85*(6), 905850612.
doi:10.1017/S0022377819000886
- Burke, A. T., Maggs, J. E., & Morales, G. J. (2000). "Experimental study of fluctuations excited by a narrow temperature filament in a magnetized plasma", *Physics of Plasmas*, *7*, 1397-1407 <https://doi.org/10.1063/1.873957>
- Shi, M., Pace, D. C., Morales, G. J., Maggs, J. E., & Carter, T. A. (2009). Structures generated in a temperature filament due to drift-wave convection. *Physics of Plasmas*, *16*(6), 062306.
- Pace, D. C., Shi, M., Maggs, J. E., Morales, G. J., & Carter, T. A. (2008). Exponential frequency spectrum and Lorentzian pulses in magnetized plasmas. *Physics of Plasmas*, *15*(12), 122304.